Wavelength demultiplexer consisting of Photonic crystal superprism and superlens

Takashi Matsumoto, Shinji Fujita and Toshihiko Baba

Yokohama National University, Department of Electrical and Computer Engineering
79-5 Tokiwadai, Hodogayaku, Yokohama 240-8501, Japan
baba@ynu.ac.jp

Abstract: We propose a novel compact wavelength demultiplexer, for which two functions arising from the anomalous dispersion characteristics of photonic crystals are combined. One is the superprism that exhibits large angular dispersion and expansion of light beam. The other is the superlens used for the focusing of the expanded light beam. Theoretically, a high resolution of 0.4 nm will be realized in the 1.55 μm wavelength range with device areas of 0.2 and 2.0 mm^2, respectively, for available bandwidths of 3 and 35 nm. Also, a low insertion loss of less than 1 dB is expected by the optimization of input and output ends of the photonic crystals. The demultiplexing function is clearly demonstrated in finite-difference time-domain simulation.

OCIS codes: (230.3990) Microstructure devices; (230.3120) Integrated optics device

References and links

1. P. P. St. J. Russell and T. B. Birks, "Bloch wave optics in photonic crystals: physics and applications," Photonic band gap materials, C. M. Soukoulis, ed. (Kluwer 1996), pp. 71-91.
2. H. Kosaka, T. Kawashima, A. Tomita, M. Notomi, T. Tamamura, T. Sato and S. Kawakami, "Superprism phenomena in photonic crystals," Phys. Rev. B **58,** R10096 (1998).
3. T. Ochiai and J. Sanchez-Dehesa, "Superprism effect in opal-based photonic crystals," Phys. Rev. B **64**, 245113 (2001).
4. T. Baba and M. Nakamura, "Photonic crystal light deflection devices using the superprism effect," IEEE J. Quantum Electron. **38**, 909-914 (2002).
5. L. Wu, M. Mazilu, T. Karle and T. F. Krauss, "Superprism phenomena in planar photonic crystal," IEEE. J. Quantum. Elecron. **38**, 915-918 (2002).
6. K. B. Chung and S. W. Hong, "Wavelength demultiplexers based on the superprism phenomena in photonic crystals," Appl. Phys. Lett. **81,** 1549-1551 (2002).
7. T. Baba and T. Matsumoto, "Resolution of photonic crystal superprism," Appl. Phys. Lett. **81**, 2325-2327 (2002).
8. T. Prasad, V. Colvin and D. Mittleman, "Superprism phenomenon in three-dimensional macroporous polymer photonic crystals," Phys Rev. B **67**, 165103 (2003).
9. B. Momeni and A. Adibi, "Optimization of photonic crystal demultiplexers based on the superprism effect," Appl. Phys. B **77**, 555-560 (2003).
10. D. Scrymgeour, N. Malkova, S. Kim and V. Gopalan, "Electro-optic control of the superprism effect in photonic crystals," Appl. Phys. Lett. **82,** 3176-3178 (2003).
11. A. V. Zayats and W. Dickson "Polarization superprism effect in surface polaritonic crystals," Appl. Phys. Lett. **82**, 4438-4440 (2003).
12. T. Matsumoto and T. Baba, "Photonic crystal ***k***-vector superprism," J. Lightwave Technol. **22,** 917-922 (2004).
13. T. Baba, T. Matsumoto and M. Echizen, "Finite difference time domain study of high efficiency photonic crystal superprisms," Opt. Express **12**, 4608-4613 (2004), www.opticsexpress.org/abstract.cfm?URI=OPEX-12-19-4608.
14. J. J. Baumberg, N. M. B. Perney, M. C. Netti, M. D. C. Charlton, M. Zoorob and G. J. Parker, "Visible-wavelength super-refraction in photonic crystal superprisms," Appl. Phys. Lett. **85**, 354-356 (2004).
15. C. Luo, M. Soljacic and J. D. Joannopoulos, "Superprism effect based on phase velocities," Opt. Lett. **29**, 745-747 (2004).
16. A. I. Cabuz, E. Centeno and D. Cassagne, "Superprism effect in bidimensional rectangular photonic crystals," Appl. Phys. Lett. **84**, 2031-2033 (2004).

#9465 - $15.00 USD Received 10 November 2005; revised 6 December 2005; accepted 7 December 2005

17. J. Witzens, T. Baehr-Jones and A. Scherer, "Hybrid superprism with low insertion losses and suppressed cross-talk," Phys. Rev. E **71**, 026604 (2005).
18. H. Kosaka, T. Kawashima, A. Tomita, M. Notomi, T. Tamamura, T. Sato and S. Kawakami, "Self-collimating phenomena in photonic crystal," Appl. Phys. Lett. **74**, 1212-1214 (1999).
19. C. Luo, S. G. Johnson, J. D. Joannopoulos and J. B. Pendry, "Subwavelength imaging in photonic crystals," Phys. Rev. B **68**, 045115 (2003).
20. E. Cubukcu, K. Aydin and E. Ozbay, "Subwavelength resolution in a two-dimensional photonic-crystal-based superlens," Phys. Rev. Lett **91,** 207401 (2004).
21. A. Husakou and J. Herrmann, "Superfocusing of light below the diffraction limit by photonic crystals with negative refraction," Opt. Express **12,** 6491-6497 (2004),www.opticsexpress.org/abstract.cfm?URI=OPEX-12-26-6491.
22. M. Notomi, "Theory of light propagation in strongly modulated photonic crystals: Refractionlike behavior in the vicinity of the photonic band gap," Phys. Rev. B **62**, 10696-10705 (2000).
23. A. Berrier, M. Mulot, M. Swillo, M. Qiu, L. Thylen, A. Talneau and S. Anand, "Negative refraction at infrared wavelengths in a two-dimensional photonic crystal," Phys. Rev. Lett. **93,** 073920 (2004).
24. J. Witzens, M. Loncar and A. Scherer, "Self-collimation in planar photonic crystals," IEEE J. Select. Topics Quantum Electon. **8,** 1246-1257 (2002).
25. X. Yu and S. Fan, "Bends and splitters for self-collimated beams in photonic crystals," Appl. Phys. Lett. **83**, 3251-3253 (2003).
26. C. Chen, G. Jin, S. Shi, A. Sharkawy and D. W. Prather, "A unidirectional photonic crystal dispersion-based emitter," Appl. Phys. Lett. **84**, 3151-3153 (2004).
27. T. Baba and D. Ohsaki, "Interfaces of photonic crystals for high efficiency light transmission," Jpn. J. Appl. Phys. **40,** 5920-5924 (2001).
28. T. Fukazawa, F. Ohno and T. Baba, "Very compact arrayed-waveguide-grating demultiplexer using Si photonic wire waveguides," Jpn. J. Appl. Phys. **43**, L673 - L675 (2004).

1. Introduction

Bulk photonic crystals (PCs) exhibit unique light propagation arising from the anomalous dispersion surface [1]. For example, the superprism phenomenon [2-17] shows a wide-angle deflection of light beam by a slight change of its wavelength and incident angle. The superlens [18-21] and the negative refractive index structure [22, 23] focus the light beam, and the supercollimator [18, 24-26] guides the light beam without expanding its width. Thus far, various applications have been expected for the superprism optics. The simplest one is a diffraction-type wavelength demultiplexer, which uses the beam deflection. However, the dispersion surface analysis indicated that the PC must be still large for getting a high resolution [7]. This constraint is caused by a large beam divergence accompanied by the beam deflection. A high resolution is rather obtained by well collimated beams under low wavelength sensitivity condition. This condition consequently requires a large PC for the spatial separation of different wavelength beams.

In a standard diffraction-type demultiplexer, the beam deflection by a grating and the beam focusing by a lens are combined to reduce the device size. Let us consider the combination of a superprism and a refractive lens, as shown in Fig. 1(a). To simplify the discussion, we first assume that input and output (I/O) ends of the superprism are parallel. Different wavelength beams deflected by the superprism reach different positions at the output end. If unwanted diffraction is suppressed at the output end, angles of output beams will be the same and parallel to the incident beam due to the $\boldsymbol{k}$ vector conservation law. Consequently, the beams are not spatially separated but condensed to one focal point by the refractive lens. Such inconvenience is originated from the essential mismatch between the superprism using the dispersion of the Poynting vector $\boldsymbol{S}$ and the refractive lens using that of the $\boldsymbol{k}$ vector. Because of this reason, we previously discussed the $\boldsymbol{k}$-vector superprism, which uses the dispersion of the $\boldsymbol{k}$ vector and the refraction at a tilted output end [12]. The $\boldsymbol{k}$-vector superprism allows a compact demultiplexer with the help of a refractive lens. However, the dispersion of the $\boldsymbol{k}$ vector is always accompanied by that of the $\boldsymbol{S}$ vector. It simultaneously changes the beam position and angle, and degrades the focused spot profile due to the spherical aberration of the lens.

#9465 - $15.00 USD Received 10 November 2005; revised 6 December 2005; accepted 7 December 2005

In this paper, we propose to combine the superprism and superlens, both of which use the ***S*** vector characteristics. As shown in Fig. 1(b), a PC with flat and parallel I/O ends is prepared as a superprism and another PC with the flat input end is placed as a superlens with a tilt angle

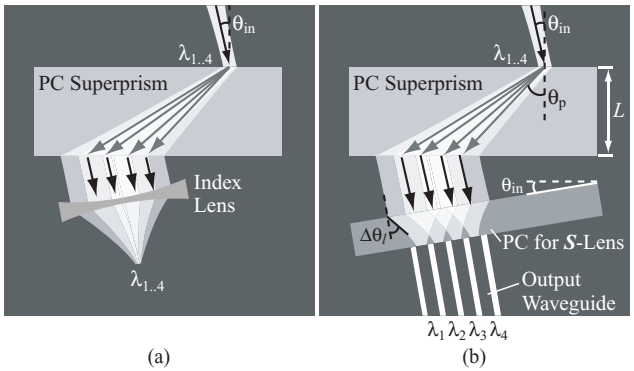

Fig. 1. Schematic of the wavelength demultiplexer consisting of the superprism and focusing lens. (a) Superprism and refractive lens. (b) Superprism and superlens.

of θ_{in} against the superprism. Light beam of a finite width is incident to the superprism with an angle θ_{in}. It is deflected and output parallel to the incident light, keeping the initial ***k*** vector. Then, it is normally incident to the superlens and focused. Absolutely different from refractive lenses, the superlens forms a real image inside the PC. Therefore, different wavelength beams are equally focused with small chromatic aberration inside the PC. The focusing characteristics are independent of the position of incident light so that the condition of the minimum spherical aberration is maintained. If the width of the focused spot is narrower than its position shift, different wavelength beams can be spatially resolved. Since the beam expansion is thus compensated by the superlens, a large angular dispersion condition of the superprism can be used, which allows a higher resolution in a smaller device size than those without superlens.

In Sections 2 and 3, we first describe the optimization of dispersion surfaces and I/O ends of the superprism and superlens. Then in Section 4, we demonstrate the wavelength demultiplexing function in finite-difference time-domain (FDTD) simulation, and discuss the relation between the resolution, device size, and available bandwidth.

2. Superprism

We have discussed the design of the superprism in Ref. [7] when it is used without lens. The optimum design that allows the highest wavelength resolution was obtained with a relatively low wavelength sensitivity. But still the beam deflection angle estimated for 4.7% frequency change is as large as 9°. It is roughly twice larger that of a standard first order diffraction grating, e.g. 600 line/mm for a wavelength $\lambda > 1.3$ μm. However, this design requires a highly collimated incident beam of $>70\lambda$ width to minimize the beam expansion inside the PC. This condition cannot be used for the superlens, because the superlens needs large angular components for focusing, and so a narrow incident beam width is rather accepted. Based on this concept, we employed the 2D PC structure and corresponding dispersion surface (contour plots of the normalized frequency a/λ over the Brillouin zone, where a is the lattice constant) of the second photonic band, as shown in Fig. 2. The 2D PC consists of airholes in a square lattice rotated by 45° with a normalized airhole diameter $2r/a$ of 0.624 and a background index n of 2.963. (We noticed in the following calculation that this lattice structure is more advantageous than a triangular lattice particularly for getting wideband operation.) The dispersion surface was calculated by using plane wave expansion method for the in-plane

#9465 - $15.00 USD Received 10 November 2005; revised 6 December 2005; accepted 7 December 2005

polarization (All the calculations in this study assumed the same polarization). The center black region shows the light cone surrounded by the air light line, which should be avoided when the superprism is fabricated into an airbridge PC slab. Vertical lines in the magnified fig. are equi-incident-angle curves indicating the dispersion characteristics for each θ_{in} [7].

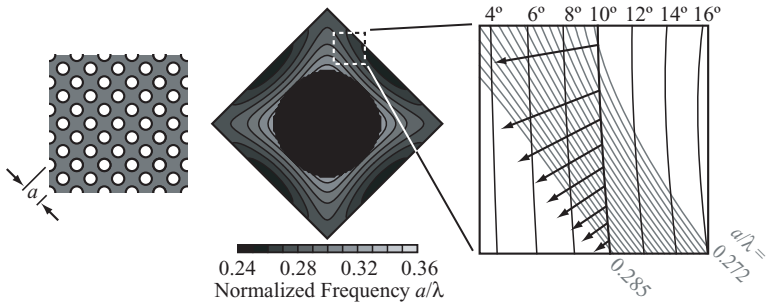

Fig. 2. Calculation model (left) and dispersion surface (right) of the superprism. Black region in the dispersion surface shows the air light cone. In the magnified fig., vertical lines are equi-incident-angle curves and gray lines are equi-frequency curves.

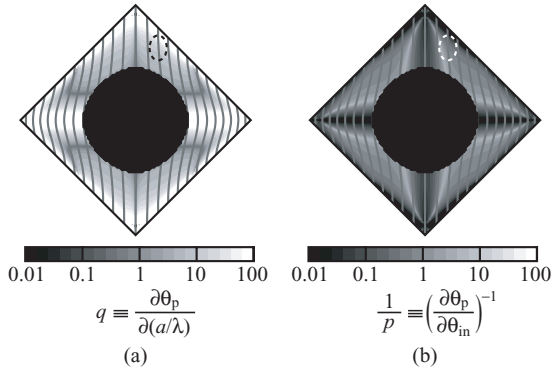

Fig. 3. Shaded drawings of two characteristic parameters for the dispersion surface of Fig. 2. (a) Wavelength sensitivity parameter q. (b) Beam collimation parameter $1/p$.

Figure 3 shows two characteristic parameters corresponding to the dispersion surface, i.e. the wavelength sensitivity parameter $q \equiv \partial \theta_p / \partial (a/\lambda)$ and the beam collimation parameter $1/p \equiv \left(\partial \theta_p / \partial \theta_{in}\right)^{-1}$ [7]. In this study, we focused on the condition near the Brillouin zone edge, at which q is three times larger and $1/p$ is six times smaller than those of the superprism in Ref. [7]. In Fig. 2, arrows indicating the $\boldsymbol{S}$ vector at $\theta_{in} = 10°$ show a wide deflection angle of 27° for 4.7% frequency change. It is roughly six times larger than that of the diffraction grating. In addition, above-mentioned $1/p$ of the superprism is still twice better than that of the grating. It is considered to be attributed to the slight deformation in equi-frequency curved, which is induced by the multi-dimensional diffraction of the superprism. Anyway, this $1/p$ is large enough to apply the superlens for focusing the expanded beam, as discussed later.

In the complete design of the superprism, the reduction in reflection loss at I/O ends is an important issue. Previously, we reported that the reflection is reduced for a wide incident beam by arranging projected airholes at boundaries of PCs [27, 13]. In this study, we further optimized the projected airholes for a narrower incident beam with wider angular components using the FDTD method. We assumed a Gaussian beam with a full width at $1/e^2$ of the peak intensity $2w_0$ of 3.22λ and a corresponding full angle of the beam divergence $\Delta\theta_{in}$ of 7.6°. Then, we finally estimated a low reflection loss of 0.2 dB/interface for a height and angle θ_t of

#9465 - $15.00 USD Received 10 November 2005; revised 6 December 2005; accepted 7 December 2005

projected airholes of 7.0r and 22°, respectively, when a/λ = 0.290 and θ_{in} = 10°. Figure 4 shows the light propagation simulated under this condition. The smooth light transmission through the PC is observed with the negative refraction and almost negligible reflection at I/O ends.

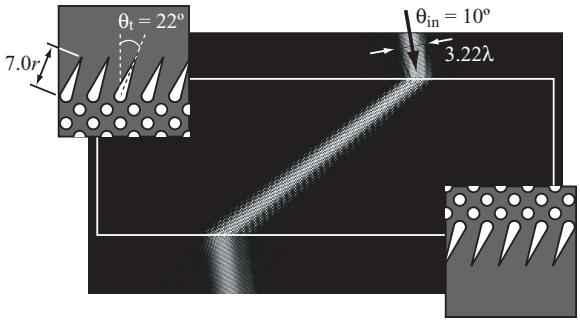

Fig. 4. Simulated intensity distribution of light propagation in the superprism with optimized I/O ends.

3. Superlens

Figure 5 shows the 2D PC structure and its dispersion surface used for the superlens. The PC consists of airholes in a deformed triangular lattice. Here, the horizontal and oblique lattice constants are denoted as a_1 and a_2, respectively, and $2r/a_1$ = 0.711 and a_2 = 0.872a_1 are assumed. The right side of Fig. 5 shows the magnified view of the dispersion surface. Arrows on the equi-frequency curve of a_1/λ = 0.306 show the focusing of the $\boldsymbol{S}$ vector by the negative refraction. In general, spherical aberration occurs in the superlens because the equi-frequency curve is slightly deformed from an ideal parabolic shape particularly for larger angular components. It results in the expanded focused spot from the diffraction limit. To suppress the aberration, we performed the ray tracing for various lattices using their dispersion surfaces. We evaluated the maximum incident angle whose ray has a focusing error smaller than a criterial length, and finally employed the structure in Fig. 5. When the criterial length was set to be λ and $2r/a_1$ = 0.711, the angle was 3.2º for the simple square lattice, while 5.2º for the structure in Fig. 5.

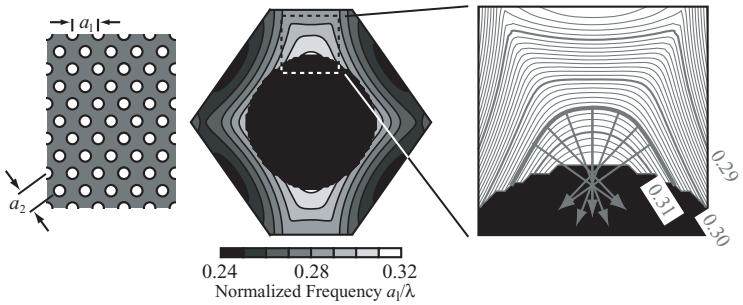

Fig. 5. Calculation model (left) and dispersion surface (right) of the superlens. Black region shows the air light cone. In the magnified fig., gray lines are equi-frequency curves. The thick one is for a_1/λ = 0.306.

In the superlens, the reflection loss must be suppressed particularly for a wide range of the incident angle. The input end was optimized for a Gaussian beam of $2w_0$ = 3.2λ, $\Delta\theta_{in}$ =7.6° and θ_{in} = 0° by the FDTD method. We found that a low loss of 0.56 dB/interface is obtained by airholes at the boundary, which have a front shape of the fourth order function of 2.8r and

#9465 - $15.00 USD Received 10 November 2005; revised 6 December 2005; accepted 7 December 2005

a triangular back shape of 0.4*r* in height. Thus, the total insertion loss will be less than 1.0 dB when the beam passes all the I/O ends of the superprism and the superlens in the demultiplexer. Figure 6 shows simulated light propagation and focused spot profile at a_1/λ = 0.306. The focused spot width $2w$ is 1.7λ at $2w_0$ = 1.0λ – 1.5λ. On this condition, $2w$ is limited by the aberration for larger angular components of the incident light. When $2w_0$ = 2.0λ – 2.5λ, $2w$ is expanded to 2.3λ – 3.0λ, respectively. It is mainly due to the diffraction limit of the ***k*** vector in the superlens. However the aberration still remains and further expands $2w$. When $2w_0$ = 3.2λ, $2w$ is 3.3λ and very close to the initial spot width, on this condition, the aberration is almost negligible. The sidelobe level decreases with the decrease in out-of focus components by the aberration.

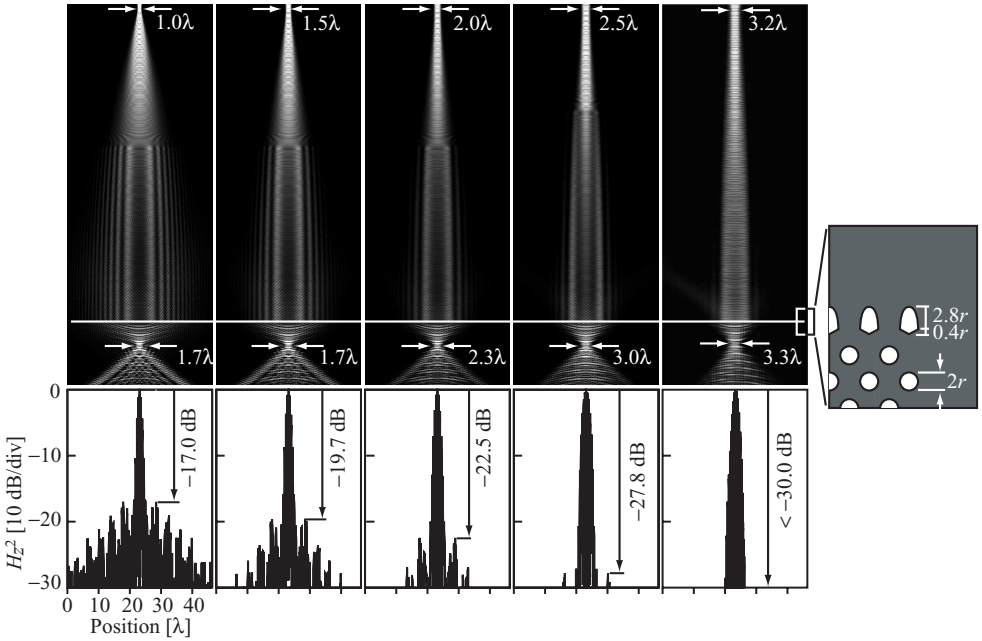

Fig. 6. Light propagation and focused spot profiles simulated in the superlens with optimized input end. Four different $2w_0$ are assumed. Disordered pattern between the excitation point and the input end of the superlens is caused by the reflected wave.

4. Wavelength demultiplexer

The demultiplexer was completely modeled, and its operation was simulated by the FDTD method. Figure 7 shows the light propagation at a/λ = 0.280, 0.284 and 0.293. The condition of incident Gaussian beam is the same as that for Fig. 4. The beam is deflected and slightly expanded by the superprism. Then, it is focused by the superlens. The unwanted reflection is well suppressed by the optimized I/O ends, and the clear and smooth light propagation is observed. In this simulation, the focused spot width $2w$ is 3.7λ for $2w_0$ = 3.2λ. When a/λ is changed from 0.280 to 0.284 and from 0.284 to 0.293, the focal point is shifted by 5λ, respectively. Therefore, the beams of different frequencies are spatially separated against the focused spot width. The crosstalk level at adjacent frequency channels could be less than −30 dB, when considering the focused spot profile in Fig. 6. Actually, however, the crosstalk was as high as −18 dB in the simulation of Fig. 7. It is thought to be caused by the slight deformation of the wavefront in the superprism, which degrades the sidelobe level of the focused spot. It will be a future important issue to be improved. In Fig. 7(b), the focal length

#9465 - $15.00 USD Received 10 November 2005; revised 6 December 2005; accepted 7 December 2005

changes from 20.8a to 11.6a for a/λ = 0.280 to 0.293. This change should be taken into account, when output waveguides are placed at focal points, as illustrated in Fig. 1(b).

The wavelength resolution demonstrated in Fig. 7 is limited by the device size assumed in this simulation. It is simply improved by lengthening the optical path in the superprism. The change of the beam deflection angle $\Delta\theta_p$ in the superprism is expressed as $q\Delta(a/\lambda)$, and

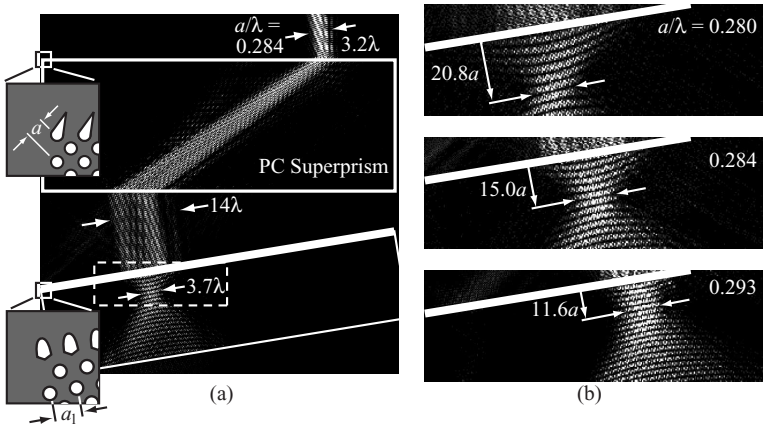

Fig. 7. Calculated light intensity distribution in the wavelength demultiplexer. (a) Total view. (b) Magnified view of the square region in (a).

the position shift of the output beam from the superprism is approximated as $q(\Delta a/\lambda)L/\cos^2\theta_p$ for the length L of the superprism. Then, $\Delta\lambda/\lambda$ is expressed as

$$\Delta\lambda/\lambda = (2w/qL)(a/\lambda)\cos^2\theta_p \tag{1}$$

where θ_p is the beam angle in the superprism, which is uniquely determined by θ_{in} and the dispersion surface. When $2w$ is not restricted by the aberration but by the diffraction limit, it is expressed as

$$2w = \alpha[\cos\Delta\theta_k/\cos\Delta\theta_{in}]2w_0 \cong \alpha(2w_0) \tag{2}$$

where α shows the beam expansion factor, and θ_k is the divergence angle of the $\boldsymbol{k}$ vector in the superlens. α is almost 1.0 only for the superlens in Fig. 6, but it is 1.16 for the superprism and superlens combination in Fig. 7. Therefore, α originates from a property of the superprism. We noticed in another calculation that α = 1.16 is kept constant when the superprism is 1.5 times longer. Thus, α is thought to be caused by the reflection of larger angular components at the I/O ends of the superprism, which effectively shows the decrease in $\Delta\theta_k$. Anyway, the fact that $2w$ is independent of the device size is very important for justifying the relation between the resolution and device size. (The relation changes if $2w$ is restricted by the aberration.) Equation (1) indicates that a high resolution is given by a large q. Figure 3 shows that $q > 40$ is obtained in the wide range of the Brillouin zone (an example is θ_{in} = 10° and $a/\lambda < 0.277$). Figure 8(a) shows $\Delta\lambda/\lambda$ calculated with q for θ_{in} = 10°, $2w_0 = 3.22\lambda$, and $L = 400\lambda$. A high resolution of $\Delta\lambda$ = 0.4 nm is obtained at λ = 1.55 μm by q = 33 for $2w = 4\lambda$.The total device area A is approximated as

$$\begin{aligned} A \cong L^2\tan(\theta_p + p\Delta\theta_{in}) + \{\tan(\theta_p + p\Delta\theta_{in}) - \tan(\theta_p - p\Delta\theta_{in})\}^2 L^2\Delta\theta_{in}/2 \\ + \{\tan(\theta_p + p\Delta\theta_{in}) - \tan(\theta_p - p\Delta\theta_{in})\}^2 L^2/2\tan\Delta\theta_l \end{aligned} \tag{3}$$

#9465 - $15.00 USD Received 10 November 2005; revised 6 December 2005; accepted 7 December 2005

where $\Delta\theta_{in}$ is given by $\lambda/\pi n w_0$ and $\Delta\theta_l$ is the focusing angle in the superlens corresponding to $\Delta\theta_{in}$. The three terms show the areas of the superprism, mid-space and superlens, respectively. This equation indicates that the device area is reduced by a large $1/p$. Figure 8(b) shows the A versus a/λ characteristics estimated from $1/p$ for $\theta_{in} = 10°$. Here, L is determined for required $\Delta\lambda/\lambda$ by using Eq. (1). Thus, L is also dependent on q. Note that A depends on how wide the total bandwidth $\Delta\Lambda$ of the device operation should be, because q and $1/p$ change nonlinearly with a/λ and particularly large q and $1/p$ are obtained in a limited bandwidth. For $2w = 4\lambda$, A = 1.3 mm^2 and 0.2 mm^2 achieve $\Delta\lambda$ = 0.4 nm at λ = 1.55 μm when $\Delta\Lambda$ is limited to 10 and 3 nm, respectively. Even if $\Delta\Lambda$ of 35 nm is required to cover the C-band of the fiber communication, A is still as small as 2 mm^2. Let us consider an ideal condition that $2w$ is reduced to 2λ by reducing $2w_0$ to ~2λ and by reducing the aberration and reflection loss. Then, A will be reduced to 0.9 mm^2 for $\Delta\Lambda$ = 35 nm. Such areas of this device are remarkably smaller than those of silica-based arrayed waveguide grating (AWG) demultiplexers and superprism demultiplexers without lens.

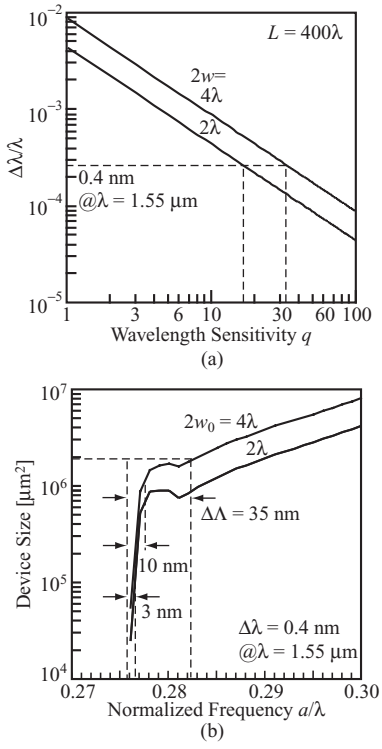

Fig. 8. Performance of the demultiplexer. (a) Normalized wavelength resolution estimated with wavelength sensitivity parameter q. (b) Device area estimated with the normalized frequency.

5. Conclusion

We proposed the compact and high-resolution wavelength demultiplexer consisting of the PC superprism for the deflection of the ***S*** vector and the superlens for the focusing of the ***S*** vector. We optimized the I/O ends of the PCs and reduced the total insertion loss to less than 1.0 dB. As a result, the wavelength demultiplexing function was successfully confirmed in the FDTD simulation. We expected a high resolution of 0.4 nm at λ ~1.55 μm by remarkably small device areas of 0.2 mm^2 and 2 mm^2 for available bandwidths of 3 nm and 35 nm, respectively. Although we used the two-dimensional calculation in this study, we expect a similar

#9465 - $15.00 USD Received 10 November 2005; revised 6 December 2005; accepted 7 December 2005

experimental result in the PC slab, because all the discussions were done under the condition below the light line.

Acknowledgments

This work was supported by The IT Program and The 21st Century COE program of MEXT, The Grant-In-Aid of JSPS and The CREST Project of JST.

#9465 - $15.00 USD Received 10 November 2005; revised 6 December 2005; accepted 7 December 2005